Nonmodel-based bioluminescence tomography using a machine-learning reconstruction strategy: supplementary material

YUAN GAO,[1,2,†] KUN WANG,[1,2,†,*] YU AN,[1,2] SHIXIN JIANG,[1,3] HUI MENG,[1,2] AND JIE TIAN[1,2,4,*]

[1]*CAS Key Laboratory of Molecular Imaging, Institute of Automation, Chinese Academy of Sciences, Beijing 100190, China*
[2]*The University of Chinese Academy of Sciences, Beijing 100049, China*
[3]*School of Computer and Information Technology, Beijing Jiaotong University, Beijing, 100044, China*
[4]*Beijing Advanced Innovation Center for Big Data-Based Precision Medicine, Beihang University, Beijing, 100191, China*
Corresponding author: kun.wang@ia.ac.cn, tian@ieee.org

This document presents the supplementary details to "Nonmodel-based bioluminescence tomography using a machine-learning reconstruction strategy," https://doi.org/10.1364/OPTICA.5.001451.

This document presents the supplementary details in the main manuscript. The Section S1 presents the details of the sample set collection. Section S2 presents the optical parameters of different organs in a mouse head. Section S3 shows the network structure of the inverse problem simulation (IPS) method. The quantitative analysis of Experiment 2 and 3 in the manuscript are presented in the Section S4. Section S5 presents the anti-noise evaluation of IPS method in dual-source reconstruction. Section S6 shows the details of IPS for *in vivo* BLT reconstruction, and Section S7 gives the discussion.

S1. Sample Set Collection

The sample set, which contains both given surface photon φ and true bioluminescent source x_{tr}, is collected by Monte Carlo (MC) simulation (MOSE v2.3) [1]. The sample collection follows two primary criteria as follows:

1) The standard mesh utilized in the MC simulation should be as similar as real mouse models in general to minimize the potential registration error.

2) The source position set, which contains all bioluminescent sources utilized in MC simulation, should cover the brain space as much as possible, with gaps in between as small as possible, as real glioma tissues can be anywhere inside the brain.

To meet the Criterion 1, the standard mesh was obtained from the segmented X-ray CT data of a female BALB/c nude mouse (4-6 weeks old), which is quite closed to the mice bearing orthotopic glioma tissues in their brains. The raw CT data for constructing the standard mesh was acquired using a pentamodal imaging system developed in our laboratory (Fig. S1) [2]. During the imaging acquisition, the mouse was anesthetized with isoflurane–oxygen mixed gas (500ml/min, Matrx VMR Small Animal Anesthesia Machine, Matrx, USA) and placed in a fixed position on the animal bed.

The BLI-CT-MRI triple modality imaging of glioma bearing mouse models also adopted the same protocol.
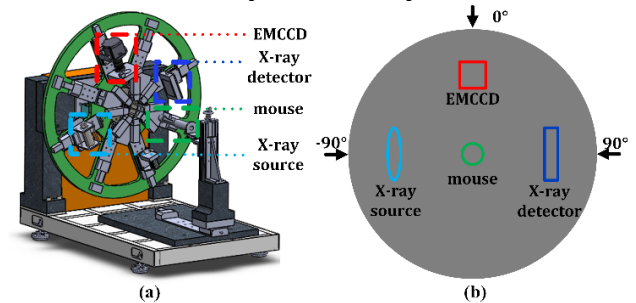

Fig. S1. The pentamodal imaging system. (a) The schematic structure of the pentamodal imaging system. (b) The physical layout of the major components for the bioluminescence and CT imaging acquisition.

To meet the Criterion 2, we simulated a single bioluminescent round source in 400 locations inside the brain. The interval distance between two adjacent tumors was set to be 0.5 mm, which is reasonably small enough considering the size of a real glioma normally ranges from 2 mm to 5 mm. The details of single round source locations are listed in Table S1. Furthermore, the MC simulation was performed eight times for each source location to collect the randomness during the photon propagation.

Table S1. Details of the single source in different locations

Radius	0.4 mm
Interval distance	0.5 mm
Maximum Photon Depth	5.4 mm
Minimum Photon Depth	1.6 mm

However, the sample set with only the single round source is not enough to train the IPS method for accurate BLT reconstruction, as real glioma tissues are far more complicated (e.g. multiple sources and irregular morphology). In order to overcome this problem without increasing the computational cost dramatically, we proposed a data-assembly method for data augment to enlarge the sample set. The idea is randomly assembling multiple single round sources with different locations, so that the sample set was extended with more complex and diverse cases.

The data-assembly method randomly selected K (2≤K≤4) samples from different locations of the single round source to construct a more complex type of bioluminescent source. Finally, we assembled 4500 new cases, which is more than 11 times of the 400 cases of the single round source located differently inside the brain.

S2. Network Structure

The IPS method contains four hidden layers, one input layer and one output layer (Fig. S2). The network input is the density of surface photon ϕ, and the output is reconstructed bioluminescence source x. The permissible region is limited in brain [3, 4], and the number of units in each layer is equal to the number of nodes in the permissible region (3265 nodes). The relationship between layer j and its next layer (layer k) is a nonlinear conversion and is expressed as

$$x^k = dropout(\text{ReLU}(B_k + W_{j,k}x^j)) \qquad (1)$$

where W_{jk} is the connection weight of the dense connection and B_k is the bias. Rectified Linear Unit (ReLU) [5] is employed as the activation function following each connection, and the activation threshold is $\lambda=0$. A dropout function (probability = 20%) is used to reduce the overfitting problem of the network [5].
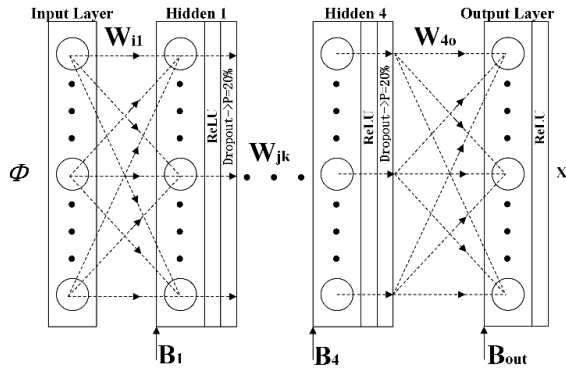

Fig. S2. The detail structure of IPS method.

To investigate the influence of IPS method with different structures, networks with different numbers of hidden layers and different dropout probabilities were evaluated in Experiment 1. Fig. S3(a) shows the performance of the IPS method with different dropout probabilities. The network with dropout probability of 0.2 provides results with the lowest mean BCE. Compared with the other probabilities, the number of samples (BCE>0.25) reconstructed by IPS with dropout probability of 0.2 is also the lowest. Fig. S3(b) shows that the network with four hidden layers performs

better in terms of both maximum and mean BCEs. The numbers of samples for BCE>0.25 and BCE>0.5 are also less than those of the other hidden layer.
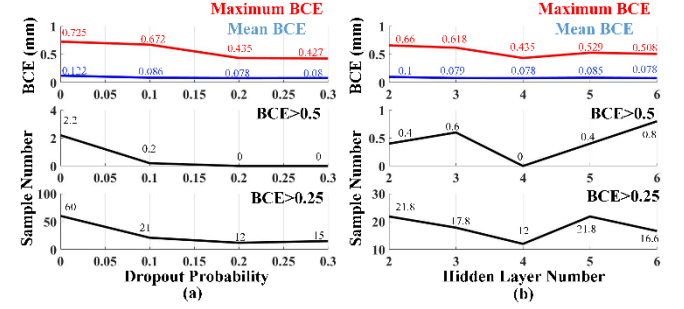

Fig. S3. Quantitative analysis of IPS method with different dropout probability and hidden layer number. (a) presents the performance of IPS with different dropout probability and (b) presents the performance with different hidden layer number

S3. Optical Parameters

The standard mesh was constructed from a segmented computerized tomographic scanning (CT) of mouse head, which contains the skull, scalp, brain and cerebrospinal fluid region. The corresponding optical parameters (680nm) [6] are listed in Table S2. [7]

Table S2. Optical Parameters of the related organs in Monte Carlo simulation

Organ	μ_a	$(1\text{-}g)\mu_s$
Scalp	0.016	0.8
Skull	0.01	1
Cerebrospinal fluid	0.0004	0.01
Brain	0.0178	1.25

S4. Quantitative Analysis

Experiment 2 was designed to evaluate the robustness of the IPS method under different organ distribution. Table S3 lists the quantitative analysis of this experiment. With the increase in the source depth from 2.2 to 3.7mm, the maximum BCE of reconstructed source is less than 0.1 mm, and the mean BCE is 0.057mm. Although the mesh of the test samples is different from the standard mesh, the IPS reconstruction results provide accurate position of the true source.

Table S3. Quantitative evaluation of Experiment 2

Source Depth	Barycenter Error (BCE)
2.2mm	0.054mm
2.7mm	0.043mm
3.2mm	0.04mm
3.7mm	0.09mm

In the dual-source reconstruction experiment, the IPS method is compared with the fast iterative shrinkage threshold (FIST) method. Four dual-source samples with different dual-source barycenter gaps are simulated using

the MOSE platform and utilized as test samples. Fig. S4 shows the BCE of results reconstructed by different methods. For both Source 1 and 2, the BCEs of the IPS method are smaller than those in the FIST method under different barycenter gaps of the dual-source. The dual-source total BCEs of IPS method are about 61.7%-91.7% less than those of the FIST method.
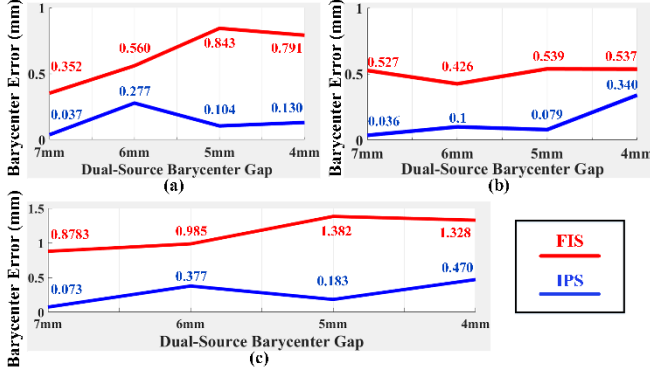

Fig. S4. Quantitative analysis of different method in dual-source reconstruction with dual-source barycenter gap from 7mm to 4mm. (a) and (b) present the BCE of reconstructed source 1 and source 2, respectively. (c) presents the total BCE of both sources.

S5. Dual-Source reconstruction with random noise

To evaluate the anti-noise performance of the IPS method, 5%, 10% and 20% Gaussian noise were applied to the dual-source study. Fig. S5 demonstrates the comparison of the dual-source BLT reconstructions using IPS and FIST with different noise levels. For each noise level, IPS provided accurate and robust reconstructions in all barycenter gap settings, but FIST failed. The quantitative analysis of the dual-source total BCEs is showed in Fig. S6. With the noise level increased from 0% to 20%, the total BCEs of IPS increased slightly. The maximal BCE was still less than 0.8 mm. The dual-source total BCEs of IPS method are about 0.54-0.92 mm, 0.50-1.18 mm, and 2.41-3.25 mm less than these of FIST in 5%, 10%, 20% noise level, respectively. These results revealed the good anti-noise performance of IPS in BLT reconstruction.

S6. *In vivo* Orthotopic Glioma BLT reconstruction

To evaluate the performance of IPS method in *in vivo* BLT reconstruction, five orthotopic glioma mouse (female BALB/c nude mice, 4-6 weeks old) models were established by green fluorescent protein (GFP) labeled U87MG-GFP-fLUC cells [8]. The raw data of CT was obtained by the pentamodal imaging system using the same protocols with the CT scanning of standard mesh in S1 section. These CT data were used as the structural imaging of each mouse, and the standard mesh was registered to each CT data, respectively [9]. The bioluminescent images were acquired by a thermoelectric cooling electron multiplying charge coupled device (EMCCD) cameras (iXonEM+888, ANDOR, UK) with multiple angles (0°, -90° and 90°, Fig. S1(b)), 20 seconds exposure and binning 4. A bandpass filter (Semrock,
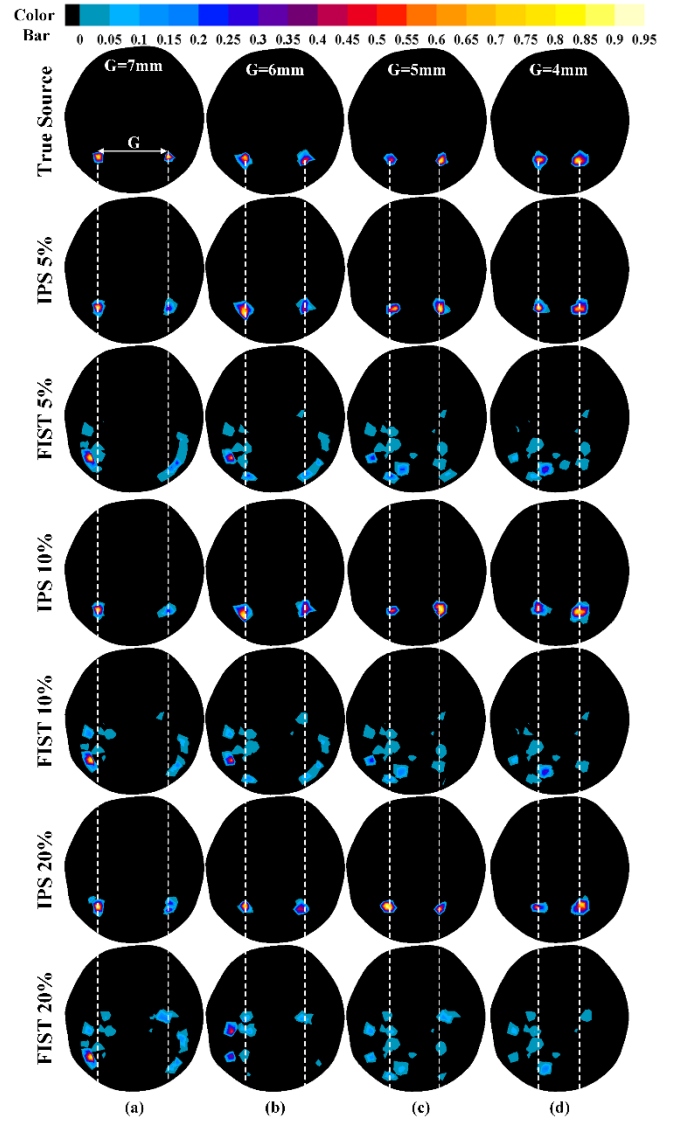

Fig. S5. Comparison of the dual-source reconstructions with different noise interferences (5%, 10% and 20%). (a) , (b) , (c), and (d) present the results in dual-source barycenter gap of 7 mm, 6 mm, 5 mm and 4mm, respectively.

USA) with 670 ± 15 nm was used at each scanning angle. The BLI raw data was mapped to their corresponding CT imaging to construct the density of surface BLI photon [10]. After that, the surface photon density was mapped to the standard mesh to construct the surface photon φ. T2-weighted MR images (M3TM, Aspect Imaging, Israel) were acquired with the following parameter: TR 6000ms, TE 50ms, slice thickness 0.7mm, and slice spacing 0.2mm.

 After the multimodality imaging acquisition, mice were sacrificed and stored in a -80°C refrigerator. Cryo-slices of each mouse head were obtained by a freezing microtome (CM 1950, Leica, Germany). The FMI scan of the tumor labeled by green fluorescent protein and the hematoxylin-eosin (H&E) staining of cryo-slices were captured by a Live Cell Imaging System (AF6000 Modular System, Leica, Germany). These *ex vivo* imaging of cryo-slices were used as the gold-standard in the *in vivo* BLT experiment.
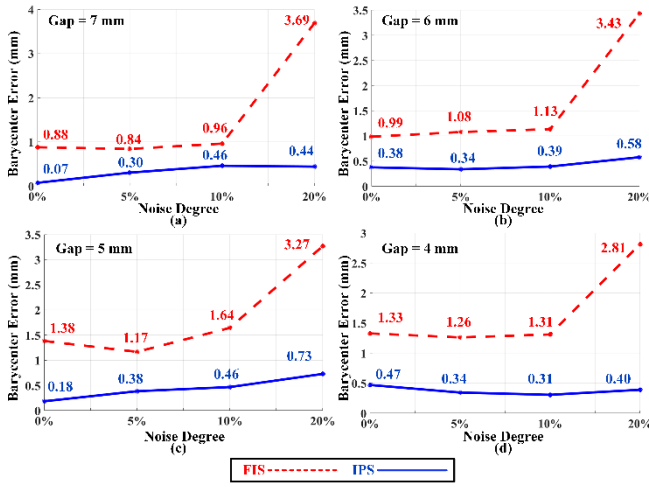
Fig. S6. Quantifications of both methods in the dual source reconstruction with different Gaussian noise levels. (a) , (b) , (c), and (d) present the results in dual-source barycenter gap of 7 mm, 6 mm, 5 mm and 4 mm, respectively.

The results of *in vivo* BLT reconstruction for five orthotopic glioma mouse models are showed in Fig. S7. Fast iterative shrinkage threshold (FIST) method [11] with diffusion equation (DE) was utilized for comparison. The tomographic slices revealed that the tumor reconstructed by FIST method were dispersedly distributed in the cranial cavity of each mouse and did not locate the region of glioma accurately. Different with FIST method, IPS-based BLT located the same region of tumor scanning from the MRI imaging. Furthermore, compared with the GFP fluorescent images and H&E staining of cryo-slices, IPS method successfully defined the tumor location of each mouse, whereas FIST method failed. The *in vivo* results of all the five mice validated the accuracy of IPD for pinpointing the tumor location in BLT reconstructions.

S7. Discussion

In this paper, we proposed a machine-learning network (MLP) based IPS method to achieve accurate and quantitative BLT reconstruction. Different with the conventional model-based method, IPS eliminated errors originated from the simplification of RTE and the ill-poseness of the model-based inverse problem. Compared with the model-based FIST method, IPS provided more accurate positioning of bioluminescent sources in both simulation experiments and *in vivo* orthotopic glioma BLT reconstructions. These results demonstrated the feasibility and accuracy of IPS for 3D pinpointing the glioma inside a living mouse.
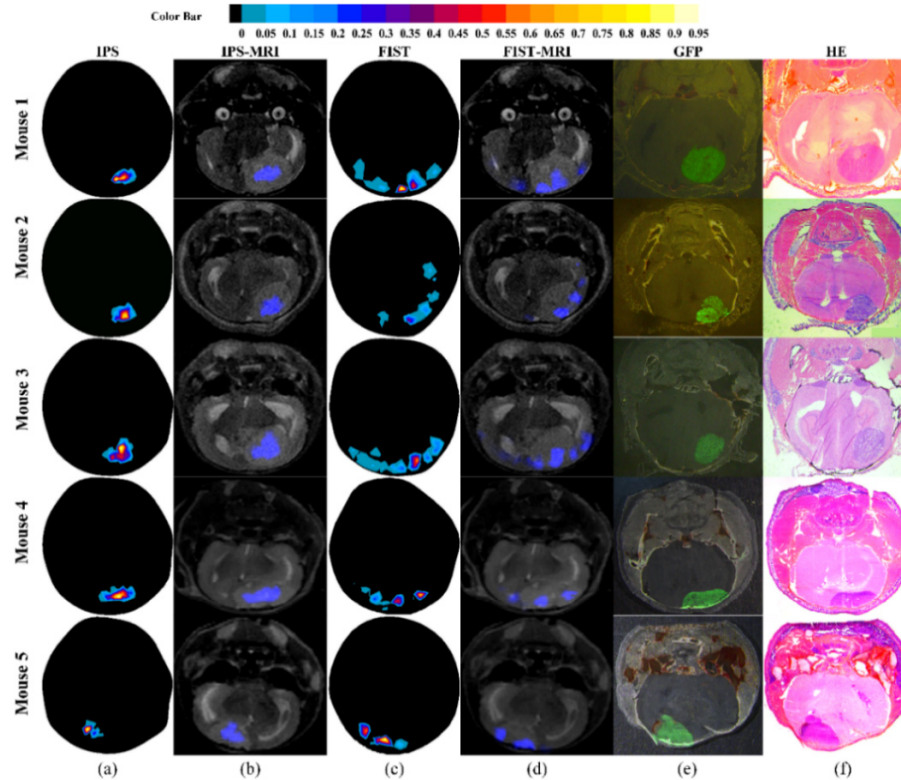

Fig. S7. *In vivo* orthotopic glioma BLT reconstruction in five mouse models. (a) and (b) The axial slice with the maximal bioluminescence source area reconstructed by IPS and its corresponding BLT-MRI fused images for each mouse. (c) and (d) Same images reconstructed by FIS. (e) and (f) The GFP fluorescence imaging and H&E staining results of cryo-slices as the gold-standard. Note: The results of FIST and IPS were reconstructed in the corresponding CT-based mesh and the standard mesh, respectively.

There are still some inherent limitations of the IPS method for in *in vivo* BLT. As a specially designed machine-learning approach, IPS is still a data driven method. Its performance highly depends on the quality of the data set used in the network training. The training data set with larger quantity and more diversity of tumors is always preferable. Therefore, for different tumors located in different organs and tissues, IPS requires tailored high quality training data sets to achieve accurate BLT reconstruction, which might be a potential obstruction for its generalized application.

In this study, the proposed strategy using MC simulation with the data-assembly method can effectively establish the training data set with remarkable smaller cost comparing to using thousands of real tumor bearing mice. However, our *in vivo* validations revealed that the current training data set based IPS was only good at tracing the glioma location, but yet lacks the accuracy of reconstructing its morphology. A better training data set with a greater variety of glioma morphology is still needed to overcome this challenge. We believe there is tremendous room for the improvement of the data augmentation method, so that the MC simulation can be better utilized to establish a more sufficient training data pool.

Last but not least, IPS also relies on a constant mesh (the standard mesh) for BLT reconstruction. Although this strategy significantly reduced the computational cost for establishing the 3D mesh of every single mouse in the training data set, which essentially empowered the practicability of IPS, it also brought the registration between the standard mesh and the real *in vivo* structural imaging (CT/MRI). This inevitably leads to an obvious drawback. For imaging brain tumor, because the brain and skull of a mouse can be regarded as rigid objects, it is not difficult to register the standard mesh to CT/MRI scans of tumor bearing mouse heads. However, it is much more difficult to employ this strategy for BLT imaging of tumors located in other organs or tissues (e.g. lung cancer, liver cancer, etc.), as such registration may induce significant bias in soft organs and tissues. Thus, an effective non-rigid registration method is crucial for the wider application of IPS, which is also one of our future works.

References

1. S. Ren, X. Chen, H. Wang, X. Qu, G. Wang, J. Liang, and J. Tian, *PloS One* 8, e61304 (2013).

2. K. Wang, C. Chi, Z. Hu, M. Liu, H. Hui, W. Shang, D. Peng, S. Zhang, J. Ye, and H. Liu, *Engineering* 1, 309-323 (2015).

3. C. Qin, S. Zhu, J. Feng, J. Zhong, X. Ma, P. Wu, and J. Tian, *Journal of Biophotonics* 4, 824-839 (2011).

4. Y. Gao, K. Wang, S. Jiang, Y. Liu, T. Ai, and J. Tian, *IEEE Transactions on Medical Imaging* 36, 2343-2354 (2017).

5. A. Krizhevsky, I. Sutskever, and G. E. Hinton, *Communications of the ACM* 60, 84-90 (2017).

6. G. Wang, H. Shen, W. Cong, S. Zhao, and G. W. Wei, *Optics Express* 14, 7852-7871 (2006).

7. G. Strangman, M. A. Franceschini, and D. A. Boas, *Neuroimage* 18, 865-879 (2003).

8. M. F. Kircher, A. de la Zerda, J. V. Jokerst, C. L. Zavaleta, P. J. Kempen, E. Mittra, K. Pitter, R. Huang, C. Campos, F. Habte, R. Sinclair, C. W. Brennan, I. K. Mellinghoff, E. C. Holland, and S. S. Gambhir, *Nature Medicine* 18, 829-U235 (2012).

9. F. Maes, A. Collignon, D. Vandermeulen, G. Marchal, and P. Suetens, *IEEE Transactions on Medical Imaging* 16, 187-198 (1997).

10. X. Chen, X. Gao, D. Chen, X. Ma, X. Zhao, M. Shen, X. Li, X. Qu, J. Liang, J. Ripoll, and J. Tian, *Optics Express* 18, 19876-19893 (2010).

11. D. Han, J. Tian, S. Zhu, J. Feng, C. Qin, B. Zhang, and X. Yang, *Optics Express* 18, 8630-8646 (2010).

Full Reference for editor and reviewers

[1]   S. Ren, X. Chen, H. Wang, X. Qu, G. Wang, J. Liang, *et al.*, "Molecular optical simulation environment (MOSE): a platform for the simulation of light propagation in turbid media," *PloS one,* vol. 8, p. e61304, 2013.

[2]   K. Wang, C. Chi, Z. Hu, M. Liu, H. Hui, W. Shang, *et al.*, "Optical molecular imaging frontiers in oncology: the pursuit of accuracy and sensitivity," *Engineering,* vol. 1, pp. 309-323, 2015.

[3]   C. Qin, S. Zhu, J. Feng, J. Zhong, X. Ma, P. Wu, *et al.*, "Comparison of permissible source region and multispectral data using efficient bioluminescence tomography method," *Journal of Biophotonics,* vol. 4, pp. 824-839, Nov 2011.

[4]   Y. Gao, K. Wang, S. Jiang, Y. Liu, T. Ai, and J. Tian, "Bioluminescence Tomography Based on Gaussian Weighted Laplace Prior Regularization for *In Vivo* Morphological Imaging of Glioma," *Ieee Transactions on Medical Imaging,* vol. 36, pp. 2343-2354, Nov 2017.

[5]   A. Krizhevsky, I. Sutskever, and G. E. Hinton, "ImageNet Classification with Deep Convolutional Neural Networks," *Communications of the Acm,* vol. 60, pp. 84-90, Jun 2017.

[6]   G.Wang, H.Shen, W.Cong, S.Zhao and G.Wei, "Temperature-modulated bioluminescence tomography," *Optics Express,* vol. 14, pp. 7852-7871, Aug 2006.

[7]   G. Strangman, M. A. Franceschini, and D. A. Boas, "Factors affecting the accuracy of near-infrared spectroscopy concentration calculations for focal changes in oxygenation parameters," *Neuroimage,* vol. 18, pp. 865-879, Apr 2003.

[8]   M. F. Kircher, A. de la Zerda, J. V. Jokerst, C. L. Zavaleta, P. J. Kempen, E. Mittra, *et al.,* "A brain tumor molecular imaging strategy using a new triple-modality MRI-photoacoustic-Raman nanoparticle,"Nature Medicine, vol.18, pp.829-U235, May 2012

[9]   F. Maes, A. Collignon, D. Vandermeulen, G. Marchal, and P. Suetens, "Multimodality image registration by maximization of mutual information," *IEEE transactions on medical imaging,* vol. 16, pp. 187-198, 1997.

[10]   X. Chen, X. Gao, D. Chen, X. Ma, X. Zhao, M. Shen, *et al.*, "3D reconstruction of light flux distribution on arbitrary surfaces from 2D multi-photographic images," *Optics Express,* vol. 18, pp. 19876-19893, Sep 13 2010.

[11]   D. Han, J. Tian, S. Zhu, J. Feng, C. Qin, B. Zhang, *et al.*, "A fast reconstruction algorithm for fluorescence molecular tomography with sparsity regularization," *Optics Express,* vol. 18, pp. 8630-8646, Apr 12 2010.